IEEE Photonics Journal
An IEEE Photonics Society Publication

Open Access

Thin-Core-Fiber-Based Long-Period Fiber Grating for High-Sensitivity Refractive Index Measurement

Volume 7, Number 6, December 2015

Cailing Fu
Xiaoyong Zhong
Changrui Liao
Yiping Wang
Ying Wang
Jian Tang
Shen Liu
Qiao Wang

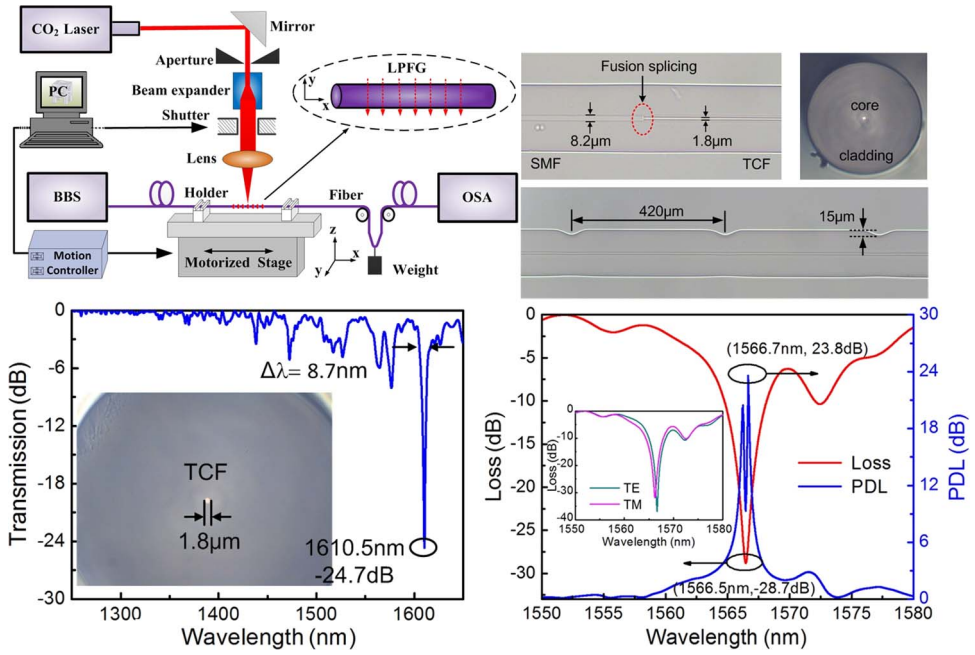

DOI: 10.1109/JPHOT.2015.2493721
1943-0655 © 2015 IEEE

Thin-Core-Fiber-Based Long-Period Fiber Grating for High-Sensitivity Refractive Index Measurement

Cailing Fu, Xiaoyong Zhong, Changrui Liao, Yiping Wang, Ying Wang, Jian Tang, Shen Liu, and Qiao Wang

Key Laboratory of Optoelectronic Devices and Systems of Ministry of Education and Guangdong Province, College of Optoelectronic Engineering, Shenzhen University, Shenzhen 518060, China

DOI: 10.1109/JPHOT.2015.2493721
1943-0655 © 2015 IEEE. Translations and content mining are permitted for academic research only. Personal use is also permitted, but republication/redistribution requires IEEE permission. See http://www.ieee.org/publications_standards/publications/rights/index.html for more information.

Manuscript received September 19, 2015; accepted October 15, 2015. Date of publication October 26, 2015; date of current version November 11, 2015. This work was supported by the National Natural Science Foundation of China under Grant 61425007, Grant 11174064, Grant 61377090, Grant 61575128, Grant 61308027, and Grant 61405128; by the Guangdong Provincial Department of Science and Technology under Grant 2014A030308007, Grant 2014A030312008, Grant 2014B050504010, Grant 2015B010105007, and Grant 2015A030310243; by the Science and Technology Innovation Commission of Shenzhen/Nanshan under Grant KQCX20120815161444632, Grant ZDSYS20140430164957664, Grant KC2014ZDZJ0008A, and Grant GJHZ20150313093755757; by the China Postdoctoral Science Foundation Funded Project under Grant 2014M552227 and Grant 2015T80913; and by the Pearl River Scholar Fellowships. C. Fu and X. Zhong contributed equally to this work. Corresponding authors: C. Liao and Y. Wang (e-mail: cliao@szu.edu.cn; ypwang@szu.edu.cn).

Abstract: We experimentally demonstrated the fabrication of asymmetric long-period fiber gratings (LPFGs) in thin core fiber by use of focused CO_2 laser beam. The proposed device exhibits a high extinction ratio of over 25 dB at the resonant wavelength and a narrowed 3-dB bandwidth of only 8.7 nm, which is nearly one order of magnitude smaller than that of LPFGs in conventional single-mode fibers. It also exhibits a high polarization-dependent loss of over 20 dB at resonant wavelength. The temperature and external refractive index (RI) sensitivity of the proposed structure are measured to be 46 pm/°C, within a temperature range from 25 °C to 100 °C, and 1047.3 nm/RIU, within the RI range from 1.400 to 1.440, respectively. The temperature induced error is ~8% for RI measurement. Such long LPFGs may find potential applications of highly sensitive RI sensors in the fields of chemical and biomedical sensing.

Index Terms: Long period fiber gratings, thin core fiber, fiber optics components, fiber optics sensors.

1. Introduction

In recent years, fiber optic refractive index (RI) sensors have attracted significant interest due to their advantages such as immunity to electromagnetic interference, small size, high sensitivity, fast response, and corrosion resistance. To date, several types of in-fiber RI sensors have been proposed, such as fiber Bragg gratings (FBGs) [1], [2], long period fiber gratings (LPFGs) [3]–[5], and fiber interferometers [6]–[10]. Among these configurations, LPFG based RI sensors are particularly attractive, since its low cost, robustness and flexibility of fabrication. However, the sensing performances of LPFGs are limited by its wide spectrum-bandwidth in practical applications. Recently, a type of thin core fiber (TCF) based optical fiber sensor has been proposed and found to be sensitive to environmental changes [11], [12]. For RI sensing, the TCF-based

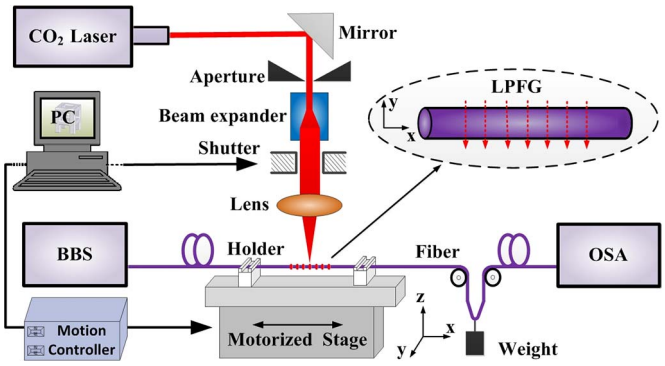

Fig. 1. Schematic diagram of the CO_2 laser system used to fabricate LPFG in thin core fiber.

fiber sensors operate with multimode interference between the fiber core and cladding modes and often need extra chemical etching or fiber-tapering techniques to improve the sensitivities.

In this paper, we demonstrate a highly sensitive fiber RI sensor based on the LPFG inscribed in the TCF. The LPFG is fabricated by periodically carve grooves on one side of the TCF by use of focused CO_2 laser beam. The obtained LPFG exhibits a large extinction ratio of 25 dB and a narrowed 3 dB-bandwidth of 8.7 nm in transmission spectrum, which is much smaller than that of LPFGs in conventional single mode fibers (SMFs). Meanwhile, the near-field mode profile and polarization dependent loss (PDL) were studied, and results show that such a LPFG exhibits a larger PDL compared with that of LPFGs in conventional SMFs. Moreover, the temperature and external-RI responses of the LPFG in TCF were also investigated, and a maximum sensitivity of 1047.3 nm/RIU can be achieved within the RI range from 1.400 to 1.440, with a temperature induced error of ~8%.

2. Experimental Details

A schematic diagram of the experiment setup is shown in Fig. 1. The light beam generated from an industrial CO_2 laser (SYNRAD 48-1, with a maximum power of 10 W and power stability of ± 2%) were delivered and focused onto fiber samples by a vibrating mirror and an infrared lens with a focal length of 63.5 mm, respectively. An electric shutter was used to control the exposure of CO_2 laser beam, and a 4× beam expander was employed to improve the focusing performance of the system. Fiber samples were mounted on a computer-controlled 2-D translation stage with a minimum step of 10 nm and a bi-directional positioning repeatability of 80 nm [13]. A small weight of ~5 g is used to provide a constant longitudinal strain on the fiber in order to help the formation of the groove during CO_2 laser heating. During the grating inscription processes, a length of 25 cm TCF (Nufern UHNA-3, with a core/cladding diameter of 1.8/125 μm) was used to avoid interferences when spliced with SMF pigtails at both ends [14]. In addition, a broadband light source (BBS) and an optical spectrum analyzer (OSA) were employed to monitor the transmission spectrum evolution of the LPFG in TCFs. The microscopic images of the splicing region and the cross section of the TCF are shown in Fig. 2(a) and (b). The fabrication processes of LPFGs in TCFs were performed as follows: 1) Scan the TCF transversely against the fiber axis with the focused CO_2 laser beam to create a notch, and then move the fiber along the fiber axis with a distance of one grating period; 2) repeat process 1) N times (N is the number of grating periods) to create a notch-formed grating; 3) repeat K cycles of process 2) to improve the notch-depth until a high-quality LPFG was obtained. The repeated scanning of the focused CO_2 laser beam induced a local high temperature in the fiber and led to the melting and gasification of SiO_2 on the surface of the fiber. As a result, periodic grooves were carved on one side of the fiber, based on which asymmetric and periodic RI modulations could be provided along the fiber axis to form a LPFG. The microscopic image of the LPFG notches is shown in Fig. 2(c), where the grating-period, notch-depth and notch-width are 400, 15 and 35 μm, respectively.

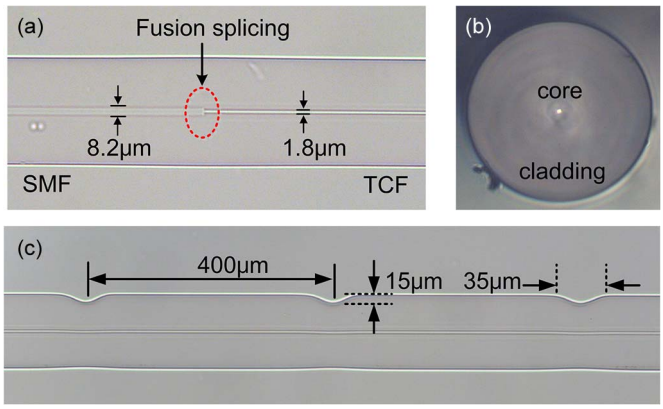

Fig. 2. Microscopic images of (a) splicing region between SMF and TCF. (b) Cross section of the TCF. (c) Periodic grooves of LPFG by focused CO_2-laser beam.

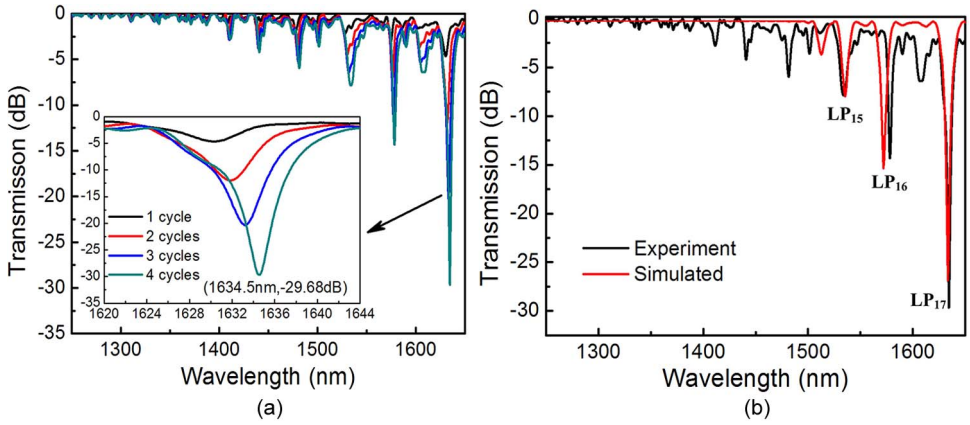

Fig. 3. (a) Transmission spectrum evolution of a CO_2-laser-inscribed LPFG in TCF with 30 grating periods and a grating period of 400 μm while the number of scanning cycles (K) increases from 1 to 4. (b) Comparison of simulated and measured transmission spectra of a TCF based LPFG with a grating period of 400 μm.

3. Experimental Results

Fig. 3(a) presents the transmission spectrum evolution of the LPFG in TCF that have shown above in Fig. 2(c) during the fabrication process. With the scanning cycle increasing, the extinction ratio of the resonant dip gradually increases and the resonant wavelength shifts toward longer wavelengths, which is opposite to that of the LPFGs in SMFs [13]. One high-quality LPFG with a large dip attenuation of −29.68 dB at the resonant wavelength of 1634.5 nm and a low insertion loss of less than 0.5 dB was achieved in TCF with only four scanning cycles. The LPFG makes the light from the fundamental mode couple to several forward-propagating cladding modes in conditions of phase-matching, and the resonant wavelength of the κth-order cladding mode is given by

$$\lambda^{(\mathrm{k})} = \Lambda\left(\mathrm{n}_{co} - \mathrm{n}_{cl}^{(\kappa)}\right) \tag{1}$$

where Λ is the grating period, and n_{co} and $\mathrm{n}_{cl}^{(\mathrm{k})}$ are the effective RI of the core mode and the κth-order cladding mode. Taking into account the grating period (400 μm), the geometry of TCF, and the refractive indices of the core and cladding materials, the transmission spectrum of a LPFG in TCF was calculated using the coupled-mode theory of the step-index fiber. The simulated and

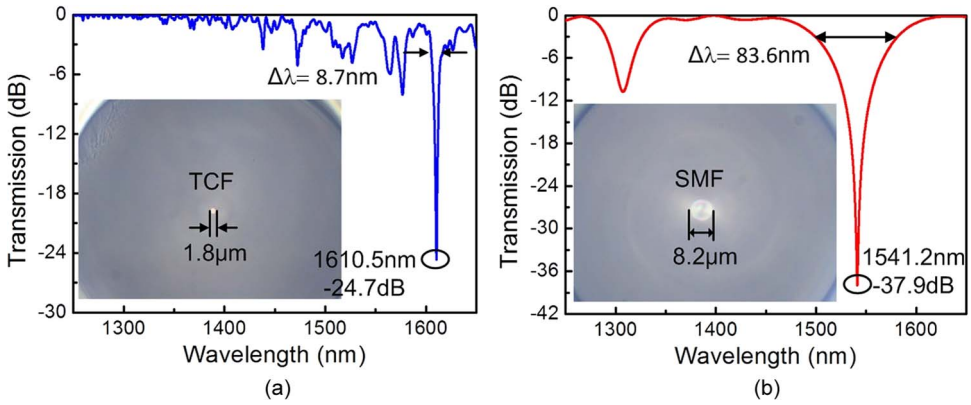

Fig. 4. Transmission spectra of LPFGs in (a) TCF and (b) SMF with same grating parameters (i.e., period: 420 μm and groove numbers: 30). (Insets) Cross section of the TCF and SMF, respectively.

experimentally measured transmission spectra are plotted in Fig. 3(b) for comparison. For convenience and clarity, only the coupling between the fundamental mode and the linear polarized (LP) LP_{15}, LP_{16} and LP_{17} modes were considered in the simulation and other lower order cladding modes that the fiber may support were ignored, which results in the differences between the measured spectrum and the simulation one at shorter wavelengths.

Note that the TCF-based LPFG shown in Fig. 3(a) and (b) exhibits a 3 dB-bandwidth of about 10 nm, which is much narrower than that of conventional SMF-based LPFGs, so we fabricated LPFGs in TCF and SMF with the same grating period (420 μm) and groove-number (30) under the same fabrication conditions for comparison. As shown in Fig. 4, the 3 dB-bandwidth of resonant attenuation dip of 24.7 dB at 1610.5 nm is only ~8.7 nm for LPFG in TCF, while the 3 dB-bandwidth of resonant attenuation dip of 37.9 dB at 1541.2 nm is ~83.6 nm for LPFG in SMFs. Obviously, the 3 dB-bandwidth of LPFG in TCF is nearly one order of magnitude smaller than that of LPFG in conventional SMFs and index-guiding PCFs, and it can be further decreased by increasing the number of grating periods. The bandwidth narrowing has been explained by [15], [16], and the 3 dB-bandwidth of LPFG may be expressed as

$$\Delta\lambda_{3\ \mathrm{dB}} \approx \frac{0.8\Lambda^2(\lambda_0)}{L}\left|\frac{d\Lambda(\lambda_0)}{d\lambda}\right|^{-1} \tag{2}$$

where L and Λ are the length and the grating period of the LPFG at the phase matching wavelength λ_0, respectively. For the TCF used here, the core is highly Ge-doped with a RI value of 1.4874. Thus, the effective RI difference between the core and cladding modes in the TCF is much larger than that in conventional SMFs. Therefore, the phase matching curves, i.e., $d\Lambda/d\lambda$, of LPFG is more steeper and exhibits a narrowed 3 dB-bandwidth than that of LPFG in SMF.

Fig. 5(a) shows the transmission spectrum evolution of the TCF based LPFG with a grating period of 415 μm. The resonant dip at ~1567.8 nm with an extinction ratio of ~31.6 dB was created after 6 scanning cycles. The near-field profiles of the fundamental core mode and the higher-order cladding mode of the LPFG are observed at 1540.2 and 1567.8 nm with the aids of an infrared camera (Model 7290A, Electro-Physics Corp.) and a microscope (Leica DM2500 M). As shown in Fig. 5(b) and (c), most power in the fundamental core mode has been excited to the circularly asymmetric cladding mode (i.e., LP_{1n}) at the resonant wavelength, which can be explained by the asymmetric RI modulation induced by the one-side-irradiation of CO_2 laser [17].

The PDL of LPFGs in TCF and SMF were also studied by the use of a PDL measurement system, which consists of a tunable laser, a photonic all-parameter analyzer, a polarization controller, and an optical power meter. Since PDL is related to the depth of the attenuation dip, two LPFGs were created with similar extinction ratios in TCF and SMF, respectively. As shown in

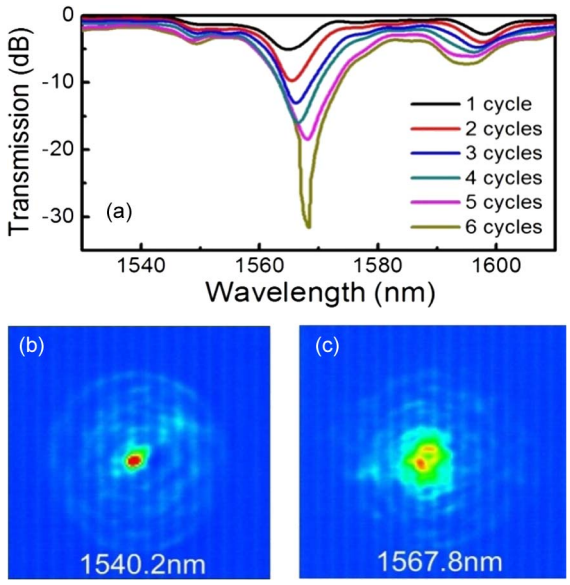

Fig. 5. (a) Measured transmission spectrum of TCF based LPFGs with a grating period of 415 μm. (b) Measured mode filed of core mode at 1540.2 nm. (c) Measured mode field of the higher order cladding mode at 1567.8 nm.

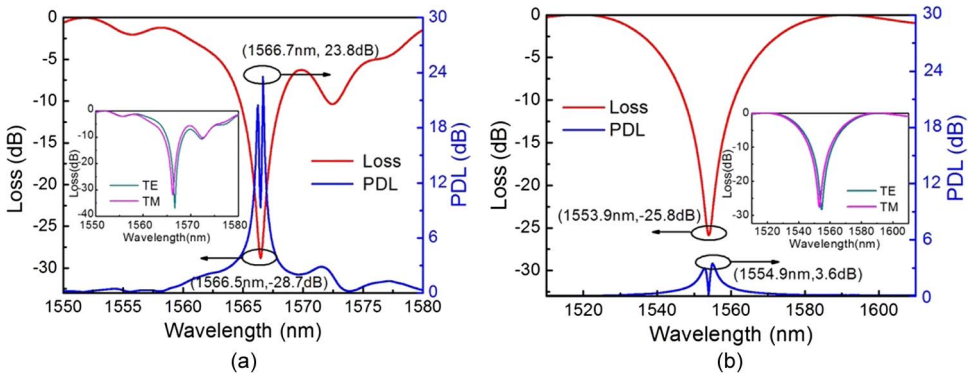

Fig. 6. Measured transmission spectrum and PDL of LPFGs in (a) TCF and (b) SMF (Inset) transmitted power of the TE and TM mode.

Fig. 6(a) and (b), the average loss and the maximum PDL of LPFG in TCF and SMF are obtained around the resonant wavelengths of 1566.5 nm and 1553.9 nm, respectively. The former exhibits a maximum PDL of 23.8 dB, which is much larger than that of the latter (3.6 dB) and those reported previously in [18], [19]. The large PDL is attributed to the significant asymmetry grooves created by the side illumination of CO_2-laser, which induced large birefringence and asymmetrical RI modulation. Since LPFGs in TCF employ the coupling between the fundamental mode and a very high order mode, such as LP_{17}, of which the power distribution spreads to the cladding more fiercely than that of LP_{16} and other lower order cladding mode. Moreover, the narrower stop band may be another reason for the large PDL, which is similar to the strong PDL of CO_2-induced LPFG on air-core PBF [16].

To compare the external RI sensing characteristic of LPFGs in TCF and SMF, two LPFGs with the same grating period and period number (i.e., 400 μm and 30) were measured at room temperature by immersing them into different RI liquids (Cargille Lab, http://www.cargille.com). After each test, the LPFG was cleaned carefully by use of alcohol to eliminate the residual liquids on the surface of fiber. As shown in Fig. 7(a), the resonant wavelength of LPFG in TCF

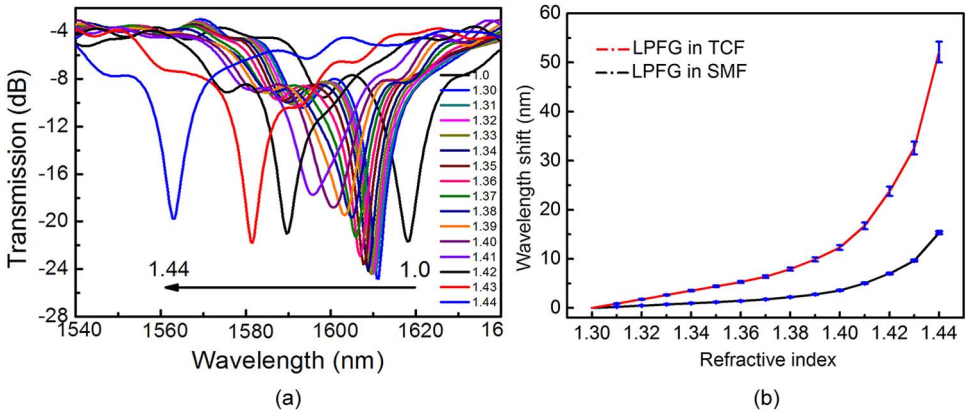

Fig. 7. (a) Transmission spectrum evolution of LPFG sample in TCF while the surrounding RI liquid change from 1.0 (air): 1.300 to 1.440. (b) Measured resonant wavelength of LPFGs in TCF and SMF versus external RI.

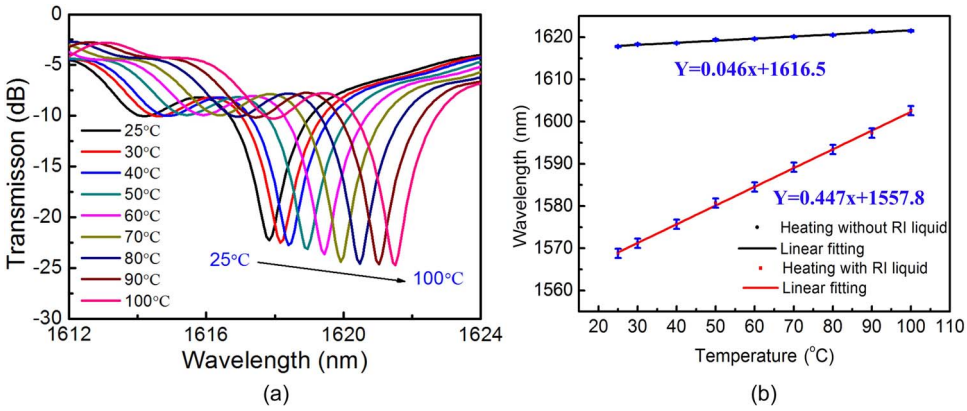

Fig. 8. (a) Measured resonant wavelength evolution of the LPFG sample in TCF while the temperature increased from 25 to 100 °C. (b) Measured resonant wavelength shift of LPFG in TCF as a function of temperature before and after immersed into RI liquid.

shifted toward the shorter wavelength with the surrounding RI increasing from 1.000 (air): 1.300 to 1.440. The measured resonant wavelength shift of LPFGs in TCF and SMF corresponding to external RI values are plotted in Fig. 7(b). It can be seen that the LPFG in TCF exhibits a resonant wavelength shift of ~54.2 nm within the RI range of 1.300~1.440, which is over 3-times larger than that of LPFG in SMF. Especially, the RI sensitivity of the former is estimated to be ~1047.3 nm/RIU in the range of 1.400~1.440. According to the heuristic formula for detection limit (DL) determination that given by White and Fan [20], [21], the DL of a RI sensor is dependent on the signal-to-noise ratio (SNR), 3 dB-bandwidth of the resonance, thermal noise and the OSA resolution. For the LPFG in TCF, DL is dominated by the 3 dB-bandwidth of the resonant dip, which is measured to be ~8.6 nm. So the DL of our sensor is estimated to be 1.73×10^{-4} for RI measurement, with assuming a SNR of 60 dB. It is believed that the RI sensitivity is mainly dependent on the cladding mode order of LPFG, and can be enhanced by reducing the cladding diameter based on tapering a fiber or etching a fiber. Hence, LPFG in TCF may excite much more higher order cladding modes (LP_{17}) than those in SMF(LP_{16}), which results in a high sensitivity of refractive index response.

To investigate the temperature influence on the RI measurement, we test the temperature response of the LPFG in TCF by putting it into a digitally controlled oven with temperature range from room temperature (25 °C) to 100 °C with a step of 10 °C. As shown in Fig. 8(a), the

resonant wavelength of LPFG in TCF shifted linearly toward longer wavelengths when the temperature increased. The measured resonant wavelength shift as a function of temperature is shown in Fig. 8(b), the corresponding temperature coefficient is ~46 pm/°C which indicates that the LPFG is temperature dependent. For comparison, the same grating was immersed into a RI liquids ($n = 1.440$ at 25 °C) and then heated from room temperature (25 °C) to 100 °C. The measured resonant wavelength shift as a function of temperature is also shown in Fig. 8(b), and the corresponding temperature coefficient is ~447 pm/°C. Account the thermal-optic coefficient of the RI liquids (-3.96×10^{-4} RIU/°C) and RI sensitivity (1047.3 nm/RIU) of the LPFG sensor in consideration, the resonant wavelength increased with a rate of 32.3 pm/°C, using the method reported in reference [11], and thus, the temperature cross-sensitivity induced error for RI measurement can be estimated to be 8%.

4. Conclusion

In conclusion, the fabrication of asymmetric groove-formed LPFGs in TCF by use of focused CO_2 laser beam is demonstrated. Such LPFGs exhibit narrowed 3 dB-bandwidth of 8.7 nm, which is nearly one order of magnitude smaller than that of LPFGs in conventional SMFs. The polarization-dependent loss of the device is over 20 dB at resonant wavelength. A temperature sensitivity of 46 pm/°C within the temperature range from 25 to 100°C and a RI sensitivity of 1047.3 nm/RIU within the RI range from 1.400 to 1.440 are obtained, respectively. The temperature induced error is estimated to be ~8% for refractive index measurement. Such long period fiber gratings may be developed as highly sensitive refractive index sensors in the fields of chemical and biomedical sensing.

References

[1] X. Fang, C. R. Liao, and D. N. Wang, "Femtosecond laser fabricated fiber Bragg grating in microfiber for refractive index sensing," *Opt. Lett.*, vol. 35, no. 7, pp. 1007–1009, Apr. 2010.

[2] M. Han, F. W. Guo, and Y. F. Lu, "Optical fiber refractometer based on cladding-mode Bragg grating," *Opt. Lett.*, vol. 35, no. 3, pp. 399–401, Feb. 2010.

[3] S. W. James, S. Korposh, S. W. Lee, and R. P. Tatam, "A long period grating-based chemical sensor insensitive to the influence of interfering parameters," *Opt. Exp.*, vol. 22, no. 7, pp. 8012–8023, Apr. 2014.

[4] T. Zhu *et al.*, "Highly sensitive optical refractometer based on edge-written ultra-long-period fiber grating formed by periodic grooves," *IEEE Sens. J.*, vol. 9, no. 6, pp. 678–681, Jun. 2009.

[5] L. Qi *et al.*, "Highly reflective long period fiber grating sensor and its application in refractive index sensing," *Sens. Actuators B-Chem.*, vol. 193, pp. 185–189, Mar. 2014.

[6] K. Misiakos *et al.*, "All-silicon monolithic Mach–Zehnder interferometer as a refractive index and bio-chemical sensor," *Opt. Exp.*, vol. 22, no. 22, pp. 26809–26819, Nov. 2014.

[7] Z. Li *et al.*, "Ultrasensitive refractive index sensor based on a Mach–Zehnder interferometer created in twin-core fiber," *Opt. Lett.*, vol. 39, no. 17, pp. 4982–4985, Sep. 2014.

[8] Y. J. Rao, M. Deng, D. W. Duan, and T. Zhu, "In-line fiber Fabry–Pérot refractive-index tip sensor based on endlessly photonic crystal fiber," *Sens. Actuators A-Phys.*, vol. 148, no. 1, pp. 33–38, Nov. 2008.

[9] Y. Wang *et al.*, "Temperature-insensitive refractive index sensing by use of micro Fabry–Pérot cavity based on simplified hollow-core photonic crystal fiber," *Opt. Lett.*, vol. 38, no. 3, pp. 269–71, Feb. 2013.

[10] J. Wu *et al.*, "Temperature-insensitive optical fiber refractometer based on multimode interference in two cascaded no-core square fibers," *Appl. Opt.*, vol. 53, no. 22, pp. 5037–5041, Aug. 2014.

[11] B. B. Gu *et al.*, "Simple and compact reflective refractometer based on tilted fiber Bragg grating inscribed in thin-core fiber," *Opt. Lett.*, vol. 39, no. 1, pp. 22–25, Jan. 2014.

[12] P. F. Wang *et al.*, "Enhanced refractometer based on periodically tapered small core single-mode fiber," *IEEE Sens. J.*, vol. 13, no. 1, pp. 180–185, Jan. 2013.

[13] X. Y. Zhong *et al.*, "Long period fiber gratings inscribed with an improved two-dimensional scanning technique," *IEEE Photon. J.*, vol. 6, no. 4, Aug. 2014, Art. ID. 2201508.

[14] B. B. Gu *et al.*, "Low-cost high-performance fiber-optic pH sensor based on thin-core fiber modal interferometer," *Opt. Exp.*, vol. 17, no. 25, pp. 22296–22302, 2009.

[15] H. Xuan, W. Jin, and M. Zhang, "CO_2 laser induced long period gratings in optical microfibers," *Opt. Exp.*, vol. 17, no. 24, pp. 21882–21890, 2009.

[16] Y. Wang *et al.*, "Long period gratings in air-core photonic bandgap fibers," *Opt. Exp.*, vol. 16, no. 4, pp. 2784–2790, 2008.

[17] Y. Wang *et al.*, "Mode field profile and polarization dependence of long period fiber gratings written by CO_2 laser," *Opt. Commun.*, vol. 281, pp. 2522–2525, 2008.

[18] M. W. Yang, Y. H. Li, and D. N. Wang, "Long-period fiber gratings fabricated by use of defocused CO_2 laser beam for polarization-dependent loss enhancement," *J. Opt. Soc. Amer. B, Opt. Phys.*, vol. 26, no. 6, pp. 1203–1208, 2009.
[19] G. Rego, "Polarization dependent loss of mechanically induced long-period fibre gratings," *Opt. Commun.*, vol. 281, no. 2, pp. 255–259, Jan. 2008.
[20] J. J. Hu, X. Sun, A. Agarwal, and L. C. Kimerling, "Design guidelines for optical resonator biochemical sensors," *J. Opt. Soc. Amer. B, Opt. Phys.*, vol. 26, no. 5, pp. 1032–1041, 2009.
[21] I. M. White and X. D. Fan, "On the performance quantification of resonant refractive index sensors," *Opt. Exp.*, vol. 16, no. 2, pp. 1020–1028, 2008.